Present-day stress profile in the Baltic Basin sedimentary succession constrained by drilling-induced structures: interpretation uncertainties

Alicja PIŁACIK[1] and Marek JAROSIŃSKI[1, *]

[1] Polish Geological Institute – National Research Institute, Rakowiecka 4, 00-975 Warszawa, Poland

A far-field stress model based on theory of elasticity and utilizing the Mohr-Coulomb criterion is commonly used in the petroleum industry as a reliable method for present-day stress profiling. We have analysed the present-day stress profile in the Lower Paleozoic shale succession of the Baltic Basin (northern Poland), based on data from a single borehole. Our analyses take into account the vertical transverse isotropy (VTI) of the mechanical properties. Initial modelling of the stress profile showed – despite general agreement concerning the length and location of the modelled and observed breakouts – systematic differences when the profile of these structures is analysed in detail. Analyses carried out for selected segments of the borehole have shown that the mere presence of breakouts affects the interpretation of the mechanical properties, and thus also the stress profile. We have analysed the size of the necessary correction for tectonic strain, to avoid this effect, as well as uncertainty resulting from the failure criteria adopted. The final model, corrected for stress disturbances by breakouts, reveals the stratification of stress regime, with the dominance of a normal faulting regime, and low values of differential stresses in the shale formations.

Key words: recent stress profile, borehole wall stability, breakouts, shale geomechanics.

INTRODUCTION

Estimation of the present-day tectonic stress field is a crucial part of the drilling operation, the importance of which became especially apparent with the development of unconventional hydrocarbons exploration. The drilling, stimulation and production processes rely significantly on proper recognition of stress orientation and magnitude. Occurrences of drilling-induced compressional failure structures (breakouts) and tensile fractures (DITF) recorded on borehole logs, provide important information about regional stress orientations (Muller et al., 1992; Zoback, 1992; Tingay et al., 2008). Together with interpretations of mechanical parameters from sonic and density logs augmented by laboratory tests, these structures can be used to determine the stress magnitude profile along the borehole axis (Zoback et al., 1985; Peška and Zoback, 1995). The method of far-field stress estimation based on a linear elastic approach and the Mohr-Coulomb failure criterion is widely used in industrial applications (Zoback, 2007; Fjær et al., 2008).

This paper describes the previously unreported phenomenon of a systematic inconsistency of the stress model with data, and discusses the credibility of the far-field stress modelling approach as applied to shale. We used industrial data from the vertical borehole OX (Fig. 1) located in the Pomeranian part of the Lower Paleozoic Baltic Basin (northern Poland) in the interior of the East European Craton, to estimate the magnitude of the present-day tectonic stress and elastic strain. Due to the significant vertical transverse isotropy of shales (Sone and Zoback, 2013), we used published elastic properties determined in both vertical and horizontal directions (Wojtowicz and Jarosiński, 2019; Wojtowicz et al., 2021; Wilczyński et al., 2021). Using this approach, we obtained the initial stress profile, that revealed a systematic discrepancy between modelled and observed breakouts. To investigate the reliability of our model, selected borehole intervals were analysed in detail utilizing alternative failure criteria. Finally, we discuss alternative solutions of the stress model and provide the results of our preferred solution.

GEOLOGICAL SETTING

The vertical OX borehole (Fig. 1) is located in the onshore Pomeranian part of the East European Craton (EEC), ~100 km away from the Trans-European Suture Zone (TESZ).
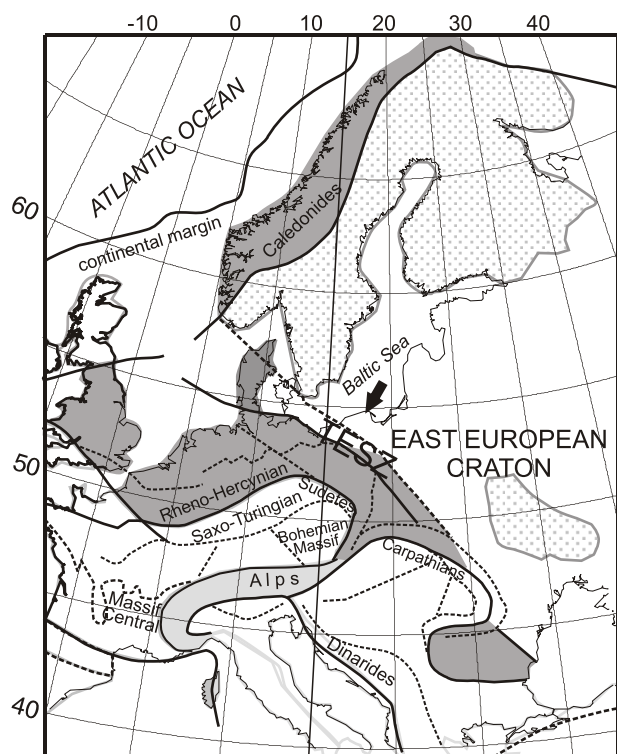
Fig. 1. Tectonic sketch map of the EEC and Paleozoic Platform contact zone (after Jarosiński et al., 2006)

Approximate location of the OX borehole marked by a black arrow, and primary (bold lines) and secondary (dashed lines) boundaries of major tectonic units; TESZ – Trans-European Suture Zone; light grey – young orogens, grey – Paleozoic Platform and orogens, dotted grey – Precambrian shields

The Precambrian basement of the study area consists of the crystalline rocks of Fennoscandia, of Paleoproterozoic age (Bogdanova et al., 2008). The OX borehole interval analysed comprises distal Cambrian passive margin deposits and Ordovician-Silurian deposits of the Lower Paleozoic Baltic Basin, being the Caledonian foredeep basin (Poprawa et al., 1999; Mazur et al., 2016). The succession consists mostly of shales and calcareous shales, in the Ordovician interbedded with limestones and marls, overlying the Cambrian sandstones at the bottom of the sequence (Modliński and Podhalańska, 2010). In the distal part of the foredeep basin analysed the shale layers are generally horizontal with limited seismic-scale tectonic deformation structures (Poprawa et al., 1999) and a regular joint system, mostly calcite-filled (Bobek and Jarosiński, 2018). The shale deposits are characterized by low permeability and generally high clay minerals content of 30–50% (Poprawa, 2020), and VTI anisotropy of elastic properties (Wojtowicz and Jarosiński, 2019; Wilczyński et al., 2021) and strength (Wojtowicz et al., 2021).

The Silurian succession is overlain directly by Permian strata, with a stratigraphic gap encompassing the uppermost Silurian, Devonian, Carboniferous and lowermost Permian. The regional context of the Devonian and Carboniferous facies distribution suggests that a significant part of the Upper Paleozoic succession was deposited and eroded during the late Variscan tectonic event (Matyja, 2006; Poprawa, 2020). After post-Caledonian erosion, deposition of >1 km of Devonian strata took place (Modliński et al., 2010; Botor et al., 2019). After exhumation in the Carboniferous, pervasive slow subsidence took place in the Permian, Mesozoic and Cenozoic, resulting in ~1 km of heterogeneous sedimentary cover (Dadlez et al., 1998).

It is a seismically stable region, in the vicinity of which two relatively strong upper crustal earthquakes of magnitudes M_W 5.0 and 5.2 were recorded on the Sambia Peninsula (Kaliningrad Oblast) in 2004 (Gregersen et al., 2007). For these, the focal mechanism solution points to a NNW–SSE orientation of maximum horizontal stress (S_H) and a strike-slip faulting stress regime (Grünthal et al., 2008). To date this is the only stress regime indicator for this part of the EEC. More stress data is obtained from borehole breakouts (Zoback, 1992). Data from three offshore and one onshore borehole closest to the OX borehole analysed by us indicate a NNW–SSE orientation of S_H, the same as from the earthquakes noted above. As demonstrated from finite elements modelling (Jarosiński et al., 2006) tectonic stresses in the Pomeranian region are constrained by the Mid Atlantic ridge push from the NW and Mediterranean collision exerting compression from the south.

DATA

In this study we applied the processed data from the OX borehole, provided by the Polish Oil and Gas Company (PGNiG S.A.), hereinafter referred to as the industrial partner. The geophysical logs cover the Lower Paleozoic succession, 1951 m in thickness. Wave Dipole Sonic, Spectral Density and micro-imager (XRMI) logs were performed by Geofizyka Toruń Co. using Halliburton tools. The elastic moduli for VTI conditions and pore pressure gradient were taken from the literature (Wojtowicz and Jarosiński, 2019) as well as unconfined compressive strength (*UCS*) (Wojtowicz et al., 2021). These mechanical parameters were determined from P-wave, S-wave and Stoneley wave velocities measured by the dipole acoustic tool, calibrated with single stage triaxial tests on vertical and horizontal samples (Wilczyński et al., 2021) and utilizing the MANNIE method introduced by Suarez-Rivera and Bratton (2012). The processed XRMI log was a source of breakout and DITF observations.

METHODOLOGY

In this study we provide a far-field stress evaluation by means of modelling the drilling-induced failure of the borehole wall, and a critical revision of results obtained based on detailed analysis of stress changes and breakout development in the most compromised intervals. All the methods used are in accordance with the theory of elasticity (Lekhnitskii, 1968; Nowacki, 1970; Jaeger et al., 2007).

FAR-FIELD STRESS DETERMINATION

Due to the basin location far from a plate boundary on a stable craton basement, with horizontal shale beds, it is reasonable to assume that one of the principal stresses is oriented ver-

tically (S_v), and in consequence the remaining two are horizontal. The vertical stress at a certain depth (z) is exerted by the overburden loading:

$$S_V = \int_0^z \rho(z)gdz \approx \bar{\rho}gz \qquad [1]$$

where: $\rho(z)$ is the overburden rock density related to depth, $\bar{\rho}$ is the mean density of a given interval, and g is the gravitational acceleration (Zoback, 2007).

The stress model was built assuming that the maximum and minimum horizontal far-field stresses, S_H and S_h respectively, are controlled by two components: (1) an overburden load, generating isotropic horizontal stress in a laterally constrained rock column, and (2) horizontal tectonic strains, ε_H and ε_h, respectively in the S_H and S_h directions. Since the horizontal shale layers reveal transverse isotropy with a vertical axis of symmetry (VTI), the equations for far-field stresses take the form (Thiercelin and Plumb, 1994; Higgings et al., 2008; Mavko et al., 2009):

$$S_h = \frac{E_h}{E_v}\frac{\nu_v}{1-\nu_h}(S_v - \alpha P_p) + \alpha P_p + \frac{E_h}{1-\nu_h^2}\varepsilon_h + \frac{E_h\nu_h}{1-\nu_h^2}\varepsilon_H \qquad [2]$$

$$S_H = \frac{E_h}{E_v}\frac{\nu_v}{1-\nu_h}(S_v - \alpha P_p) + \alpha P_p + \frac{E_h}{1-\nu_h^2}\varepsilon_H + \frac{E_h\nu_h}{1-\nu_h^2}\varepsilon_h \qquad [3]$$

where: E_h, E_v are Young moduli, and ν_h, ν_v are Poisson ratios in horizontal and vertical directions (perpendicular and parallel to the borehole axis) respectively.

In the current study we utilize the formation pore pressure (P_p) gradient approximated by Wojtowicz and Jarosiński (2019) assuming hydrostatic brine pressure, the S_v gradient provided by the industrial partner, and the mean constant value of Biot's coefficient ($\alpha = 0.7$) estimated following geophysical log analysis by Stadtmüller et al. (2017). The strain values ε_H and ε_h are variables of the stress model adjusted to results of breakout and DITF analysis. It is assumed that ε_H and ε_h are uniform for the whole borehole length analysed. This assumption is valid in particular for aseismic basins located far from plate boundaries where neither strain compartmentalization nor thin-skinned effects are expected, as in the basin analysed.

STRESS DEVIATION IN THE BOREHOLE WALL

The borehole wall is a surface of discontinuity that causes redistribution of the far-field stresses in its vicinity. That may in turn lead to borehole wall failure in the form of compressional breakouts (BO) and drilling-induced tensile fractures (DITF) (Zoback et al., 1985). The occurrences of breakouts and DITF allow for determination of the tectonic stress orientation and estimation of stress magnitudes. According to Zoback et al. (1985), Barton et al. (1988) and Zoback (2007) the formulae for breakouts and DITF can be derived from modified Kirsch equations for stress distribution around the hole in a linear elastic

medium subjected to plane strain conditions and the Mohr-Coulomb (Appendix 1*) failure criterion. The governing condition for breakout initiation at the borehole wall in the direction of the S_h azimuth is that circumferential stress $\sigma_{\theta\theta}$, reaching its maximum value there, exceeds the strength of the rock:

$$\sigma_{\theta\theta} \geq UCS_h + N\sigma_{rr} \qquad [4]$$

where: N is a function of the internal friction angle φ:

$$N = \frac{1 + \sin(\varphi)}{1 - \sin\varphi} \qquad [5]$$

The radial stress σ_{rr} on the borehole wall equals the difference between mud fluid pressure P_f and pore pressure P_p, which is usually greater than zero for shales due to the low permeability.

In our analysis we use UCS values in a horizontal direction (UCS_h). Having no direct data on internal friction angle changes we assumed a typical value of $\varphi = 25$ following analysis of boreholes from the Baltic Basin (Wojtowicz et al., 2021). The resulting equations define the conditions for breakout [eq. 6] and DITF [eq. 7] development:

$$3S_H = S_h + P_P(1 - N) + P_f(1 + N) + UCS_h \qquad [6]$$

$$S_H = 3S_h - P_P - P_f - T_0 \qquad [7]$$

where: T_0 denotes the tensile strength of the rock in a horizontal direction. The thermal stress component, while of more significance for rocks with low permeability (Wang and Dusseault, 1995) is omitted due to the lack of thermal parameter data in the current study.

By assuming that the observed width of the breakout ω_{bo} is constant and related to the steady state of stress in the borehole wall this parameter can be also used for stress calculations (Barton et al., 1988; Zoback, 2007):

$$S_H + S_h - 2(S_H - S_h)\cos(2\theta) = P_P(1 - N) + P_f(1 + N) + UCS_h$$

$$[8]$$

$$2\theta = \pi - \omega_{bo}$$

The occurrences of breakouts and DITF were used as a governing factor, when estimating values of ε_H and ε_h with the far-field stress equations [2 and 3], in choosing the best possible fit between the combined length of observed and modelled structures.

BREAKOUT ANALYSIS USING ALTERNATIVE FAILURE CRITERIA

For this study we used the Mohr-Coulomb for stress profile modelling and Wiebols-Cook (Appendix 2) and Lade-Duncan (Appendix 3) criteria for comparative analysis of breakout failure at given depths.

---

* Supplementary data associated with this article can be found, in the online version, at doi: 10.7306/gq.1620

The Mohr-Coulomb criterion, while most commonly used in borehole failure analysis, does not take into an account the strengthening effect of the second principal stress σ_{22} on the rock, which causes an overestimation of P_f required for borehole stabilization (Colmenares and Zoback, 2002; Benz and Schwab, 2008; Zhang et al., 2010). The Wiebols-Cook criterion, based on Drucker-Prager and modified by Zhou, includes a σ_{22} strengthening effect moderating the estimates. Similar results are obtained while using the Lade-Duncan criterion modified by Ewy, according to which the rock strength rises alongside σ_{22}, to drop slightly when σ_{22} reaches a given critical value (Colmenares and Zoback, 2002; Benz and Schwab, 2008; Zhang et al., 2010).

For modelling of individual breakouts using alternative failure criteria we have used a MATLAB-based code Breakout Analysis for Anisotropic Rocks (BAAR). This code was developed for two-dimensional analysis of failure zones around a pressurized borehole in an anisotropic rock subjected to far-field loads (Piłacik et al., 2017). BAAR uses an analytical solution for stress distribution around a circular hole in an orthotropic or VTI elastic medium in plane strain state, based on the complex variable method by Mushkhelishvili (Lekhnitskii, 1968; Savin, 1970). For the complete solution in Cartesian coordinates the appropriate equation for stress in a given direction σ_{ii} [eq. 9–11], where ii = xx, yy, xy, should be calculated separately for $\theta = 0$ and $\theta = \pi/2$ and then summed.

$$\sigma_{xx} = \sigma_0 \cos^2(\theta) - 2R\left[s_1^2 \zeta_1^{0'}(z_1) + s_2^2 \zeta_2^{0'}(z_2) \right] \quad [9]$$

$$\sigma_{xx} = \sigma_0 \sin^2(\theta) - 2R\left[\zeta_1^{0'}(z_1) + \zeta_2^{0'}(z_2) \right] \quad [10]$$

$$\sigma_{xx} = \sigma_0 \sin(\theta)\cos(\theta) - 2R\left[s_1^2 \zeta_1^{0'}(z_1) + s_2^2 \zeta_2^{0'}(z_2) \right] \quad [11]$$

where: σ_0 is the far-field stress in a given direction. For the sake of simplicity, it is assumed that the S_H azimuth is equal to $\theta = 0$ (along the x-direction). The ζ_1^0 are modified stress functions (Lekhnitskii, 1968; Savin, 1970), s_i are complex roots of the equation:

$$\frac{1}{E_1} s^4 + \left(\frac{1}{G_{12}} - 2\frac{\nu_{12}}{E_1} \right) s^2 + \frac{1}{E_2} = 0 \quad [12]$$

and z_i are complex functions of s_i. For VTI medium:

$$E_1 = E_h \qquad E_2 = E \qquad \nu_{12} = \nu_h \qquad G_{12} = \frac{E_h}{2(1+\nu_h)} \quad [13]$$

where: G_{12} is shear modulus.

Borehole stability is assessed in BAAR in a comprehensive analysis by multiple failure criteria. Depending on the configuration of available parameters, BAAR can be used for estimation of multiple variables. With prior knowledge of the elastic moduli, UCS, ω_{bo} and P_f the criteria presented can be applied to investigate stress conditions required for the occurrences of breakouts of given size. If one of the horizontal stresses is also known or assumed, the magnitude of the other one and the differential stress can be also estimated. The same method can also be used for breakout-free intervals, to evaluate the stability conditions.

BOREHOLE STABILITY ANALYSIS FOR STRESS ESTIMATION

DRILLING-INDUCED FAILURE

According to the XRMI log interpretation the breakouts in the OX borehole are developed irregularly. In addition to clearly distinguishable rows of spallation located on opposite sides of the borehole wall, there are multiple intervals of 10–30 cm high chippings, often associated with the bedding geometry or regular tectonic fractures. Sometimes, it is difficult to correlate breakouts on both sides of the borehole wall in those intervals, and sometimes only one side is spalled. Additionally, the breakouts angular widths vary significantly, also within the correlated pairs. Due to the irregularity of the breakouts, the cumulative length of those structures is determined somewhat subjectively. By applying not overly restrictive criteria for the similarity of breakout geometries on both sides of the borehole wall, the total length of regular breakouts in the OX borehole was estimated at ~99 m.

All observed breakouts occur in the uppermost Silurian Puck Formation. Despite the considerable heterogeneity of breakout geometry, they exhibit a stable azimuth orientation that is statistically 61 ±20°. Therefore, they mark a NNW–SSE direction of S_H, which is consistent with the existing observations and models for this part of the EEC (Jarosiński, 2005, 2006; Jarosiński et al., 2006). Several-metre-long DITF were observed in the wall of the lower part of the borehole, in the Sasino Mudstone Formation. Additionally, in the core obtained from this formation, centerline fractures were found, which are also induced by drilling fluid pressure and localized below the current bottom of the borehole. Centerline fractures interfere here with tectonic fractures of a similar orientation (Bobek and Jarosiński, 2018). We had no core available from the lowest, Cambrian interval of the OX borehole, but in the adjacent borehole OX-2, centerline fractures were observed also at the Cambrian level. We used these observations to evaluate the results of modelling of the contemporary stresses.

MODELLING OF TECTONIC STRAIN AND STRESS

Our stress analysis includes the initial estimation of horizontal stress and strain by means of modelling of the theoretical breakout profile, followed by comparison of the modelled and observed breakouts, analysis of mechanical context of breakout development and final correction to the initial stress and strain estimation. The theoretical breakout profile was modelled using the horizontal stresses assessed from the formulae [eq. 2 and 3]. The tectonic strains ε_H and ε_h in the directions of principal stresses S_H and S_h were assumed to be constant along the entire borehole profile analysed. The far-field stresses obtained were used to calculate stress concentration and relaxation in the borehole wall using the formulae [eq. 6 and 7]. The comparison of stress distribution at the borehole wall with the UCS_h and T_0 allowed us to predict the development of breakouts and DITF. The width of breakouts was also calculated but, due to the irregularity of the observed breakouts, was not used for model evaluation. The resulting stress magnitudes were used

to model breakouts and DITF, which were then juxtaposed with the failure structures observed on the XRMI logs BO_X and $DITF_X$. To evaluate the modelling results we compared the combined length of modelled breakouts (BO_M) and DITF to these observed (BO_X) and their relative position in the borehole. We used a trial and error procedure of fitting the model to observations using breakout length as the only quantitative fitting parameter.

As a general rule, the total length of BO_M increases alongside the maximum strain (contraction/shortening is positive). The increase in ε_H causes an increase in S_H magnitude and in consequence a rise of maximum tangential stress $\sigma_{\theta\theta}$ at the borehole wall. Because the lowest stress in this case is the borehole mud fluid pressure P_f, constant at given depth, the differential stresses also increase alongside the $\sigma_{\theta\theta}$. Thus, by adjusting ε_H we were able to control the fitting of breakout lengths in the most direct way, checking their placement in the borehole profile. Excessive increase of ε_H caused the BO_M to spread beyond the length range of the observed ones, and insufficient ε_H caused the BO_M to be sparse and overly short. Thus, the result of our modelling is a compromise between fitting of breakout lengths and adjusting their range. In turn, the ε_h most affects the magnitudes of S_h and minimum $\sigma_{\theta\theta}$ at the borehole wall, which controls the formation of the tensile fractures DITF. Because in the OX borehole such structures occur only in the lower parts of the profile, in the Sasino and Cambrian formations, the ε_h was adjusted such that the model fits this condition.

According to equations 2 and 3, the ε_H and ε_h strains affect each other, which has, however, a secondary effect on the spreading of BO_M. The magnitude of far-field differential stress (S_H–S_h) is also an important factor as its increase causes the formation of breakouts with a more uniform width, and promotes the formation of DITF.

We then proceeded to adjust ε_H and ε_h to obtain the most fitting overlap of modelled and observed failure zones along the borehole length (Fig. 2). The above procedure was repeated to obtain S_H and S_h magnitudes (Fig. 2). As result, we estimated ε_H and ε_h to be equal:

$$\varepsilon_h = 0.00014 \text{ and } \varepsilon_H = 0.00056 \qquad [14]$$

Due to the method of the estimation, the strain magnitudes should be treated as of high uncertainty. The total length of BO_M is 98.5 m and is almost equal to the total length of BO_X, estimated at ~99 m, which proves a rather accurate fit between model and observations (Fig. 2). The highest concentration of BO_M was obtained in the lower interval of the Puck Formation (Figs. 2 and 3) which generally fits the range of BO_X. In comparison to the underlying breakout-free Kociewie Formation, the interval with BO_M is characterized by lower average magnitudes of UCS_h, S_H and S_h (Fig. 2). The lower value of UCS_h is expected since the weakening of the rock promotes breakout formation. However, when we zoom into the borehole interval with breakouts, we can see that the sections with BO_M and sections with BO_X miss each other quite systematically (Fig. 3).

As such, while our model effectively estimates the length and range of the breakout sections, it does not deliver a good fit when it comes to the individual breakouts. We observed that for, the majority of BO_X sections, horizontal stresses decrease instead of increasing (Fig. 3), which is inconsistent with breakout formation conditions. This might be the reason why BO_M do not form even with UCS_h values being lower or comparable in those intervals.

INCONSISTENCY BETWEEN MODELLED AND OBSERVED BREAKOUTS

We examined the systematic discrepancy between the occurrence of observed and modelled breakouts on selected, typical intervals of the OX borehole, in which BO_M and BO_X occur and only partially overlap (Figs. 4 and 5). The ULTRA mineral composition processing results for this section of the OX borehole show that the breakouts observed preferentially occur in layers with increased carbonate content, which rises from ~5–10% to reach 30%. Although this correlation is not strict, such a lithological change should affect the mechanical properties, which should explain to some extent the stress concentration in the layers with the observed breakouts. According to the mechanical model adopted by us, with a relatively stable value of UCS_h and P_f, in order for a breakout to initiate in a given section, the magnitude of the S_H should increase in relation to the section without breakouts. While, in the OX borehole, the S_H decreases fairly regularly in the sections with BO_X (Figs. 3–5).

To investigate this phenomenon, we calculated the average values of horizontal stresses for BO_X and BO_M sections in upper (U) and lower (L) test intervals (Figs. 4 and 5), and compared them with average values for background, i.e. breakout ree, zones (Fig. 6). We observed that for the BO_X sections the stress magnitudes are inconsistent with breakout formation conditions. The total length of BO_X in the upper interval is 19.7 m, 99% of which are breakout sections with inconsistent S_H magnitudes. In those sections, values of S_h are lower than background for ~0.2–9.5% with an average of 10%, with an exception of 7% of those sections total length where values of S_h are higher than average for background. The values of S_H are lower than background for ~2.3–22% with an average of ~12%. The BO_M sections are of total 5.1 m length, where magnitudes of S_h are higher than background for ~7.8–2.2% with an average of ~13.4% and magnitudes of S_H are higher than background for ~6.6–0.7% with an average of ~12.1%. The BO_X and BO_M overlap for 2.9 m, which is ~14.7% of total BO_X length and 56.9% of BO_M length. The total length of BO_X in the lower interval is 13.1 m, 100% of which are breakout sections with inconsistent S_H magnitudes. In those sections values of S_h are lower than background for ~1.3–8.6% with an average of ~10.5%, with an exception of 1.5% of those sections total length where values of S_h are higher than average for background. The values of S_H for BO_X are lower than background for ~0.6–1.9% with an average of ~12.6%.

The BO_M sections are of total 9.5 m length, where stress magnitudes are higher than background for ~5.7–0% for S_h with average 13.5% and for ~2.9–8.6% for S_H with average 12.3%. There is only one 0.6 m-long BO_M section where stress changes are inconsistent with breakout formation conditions and vary from background by 1.8% for S_h and by 4% for S_H, which might be due to the averaging of the background parameters values. The BO_X and BO_M overlap for 3.8 m which is ~29% of total BO_X length and 40% of BO_M length. For both intervals, only 0.5 m of BO_X sections with stress magnitude changes consistent with breakout formation conditions overlap with BO_M.

The comparison above clearly shows that in the borehole intervals with visible breakouts, stress changes do not favour failure of borehole wall. As with the constant strain in the borehole profile, the magnitude of stress is determined by the mechanical properties; therefore, we formulate a hypothesis that
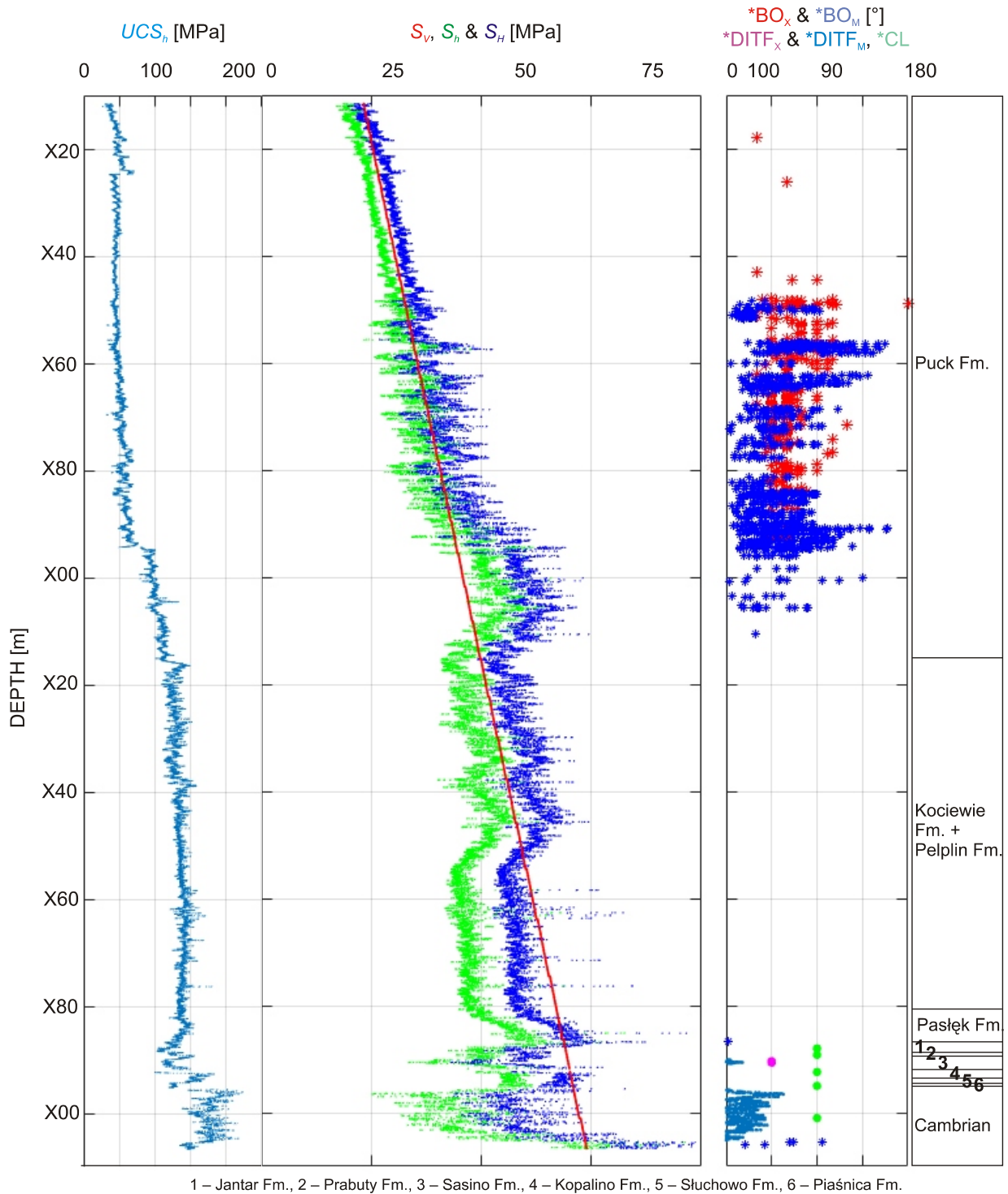
1 – Jantar Fm., 2 – Prabuty Fm., 3 – Sasino Fm., 4 – Kopalino Fm., 5 – Słuchowo Fm., 6 – Piaśnica Fm.

Fig. 2. Stress profiles obtained by fitting the length of modelled and observed breakouts

The first plot shows the USC_h profile for borehole OX as obtained by Wojtowicz et al. (2021). The second plot depicts the S_V profile derived from [eq. 1] and the modelled profile of S_H and S_h estimated using a far-field stress approach, for minimum and maximum elastic strains $\varepsilon_h = 0.00018$ and $\varepsilon_H = 0.00056$, respectively In the last column the observed (BO_X) and modelled (BO_M) breakouts, observed ($DITF_X$) and modelled ($DITF_M$) drilling-induced tensile fractures, and centerline fractures (CL), are shown

the inconsistency between observed and modelled breakouts is caused by the BO_X themselves, since the failure of borehole wall might influence interpretation of mechanical properties from the geophysical logs. Due to the repeated inconsistency in

BO_X and BO_M intervals we decided to change the stress model to the level at which BO_M disappear from BO_X-free intervals. But, prior to this we checked what differences in the magnitude of stress may result from adopting different failure criteria.
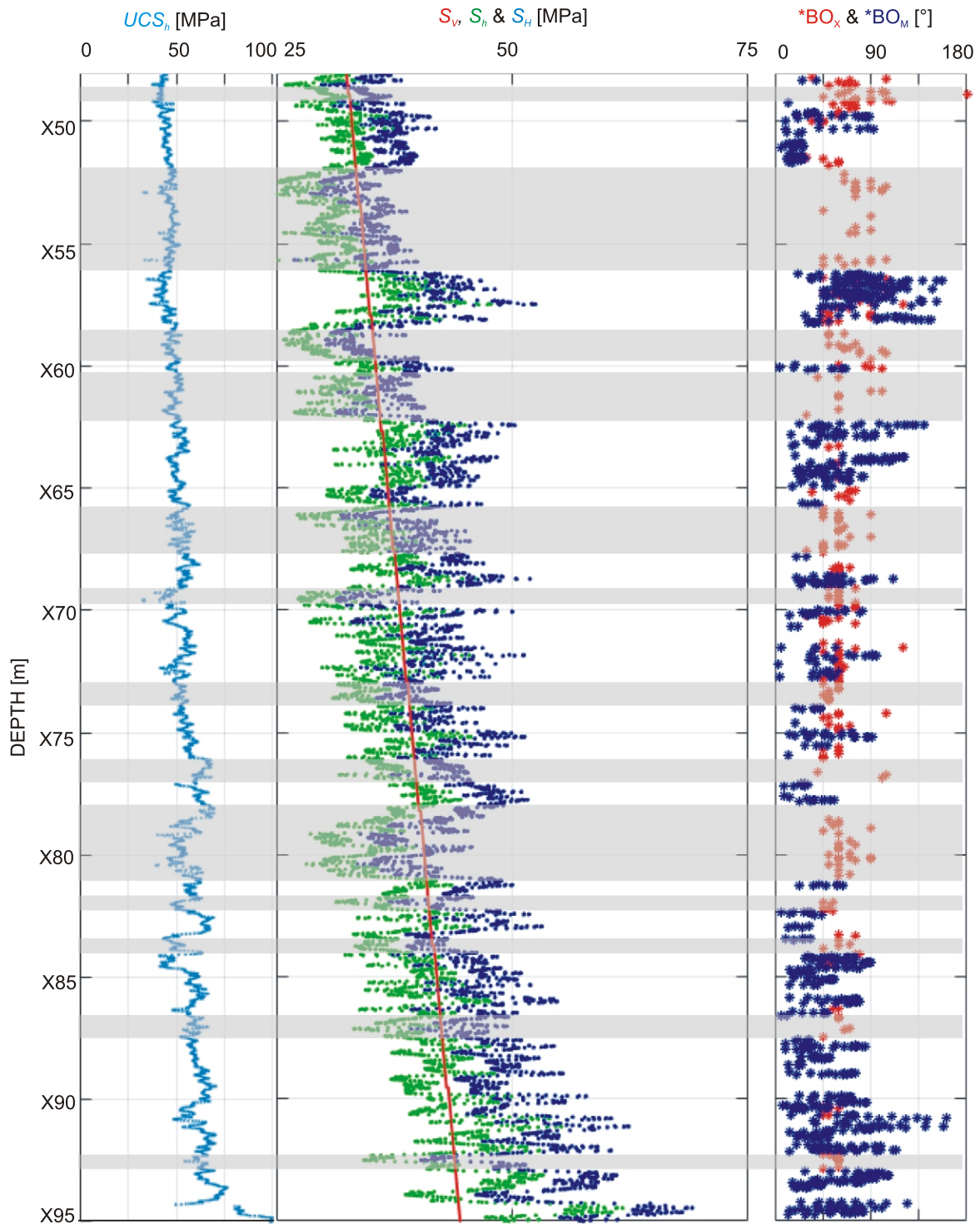
Fig. 3. Zoom of the borehole interval with breakouts, showing the fit of the observed and modelled breakouts

The first plot shows the USC_h profile for the borehole OX interval with breakouts (lower Puck Formation) as obtained by Wojtowicz et al. (2021). The second plot depicts the S_V profile derived from [eq. 1] and the modelled profile of S_H and S_h estimated using a far-field stress approach, for ε_h = 0.00018 and ε_H = 0.00056. In the last column the observed (BO_X) and modelled (BO_M) breakouts are shown. The grey fields mark the exemplary BO_X intervals for which BO_M did not occur
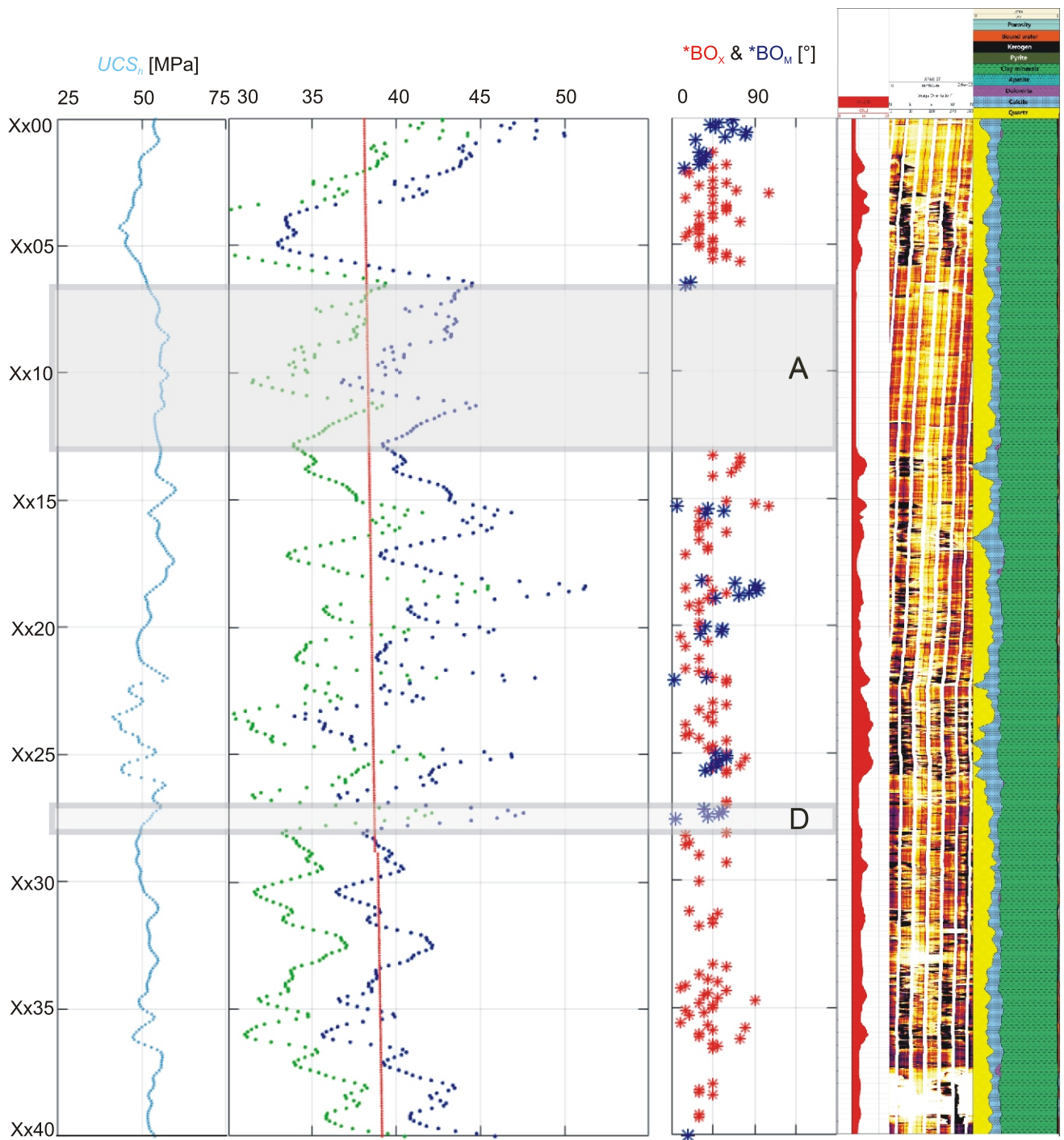
**Fig. 4. Integrated model of strength and stress profiles with observed and modelled breakouts
from the upper selected depth interval**

The first plot shows the UCS$_h$ profile for the borehole OX upper test interval with breakouts (lower Puck Formation) as obtained by Wojtowicz et al. (2021). The second plot depicts the S_V profile derived from [eq. 1] and the modelled profile of S_H and S_h estimated using a far-field stress approach, for ε_h = 0.00018 and ε_H = 0.00056. In the third column the observed (BO$_X$) and modelled (BO$_M$) breakouts are shown. The last column consists of caliper and XRMI logs and the lithological profile. The frames show the representative BO$_X$-free and BO$_M$-free interval A and BO$_X$-free interval D where BO$_M$ occur
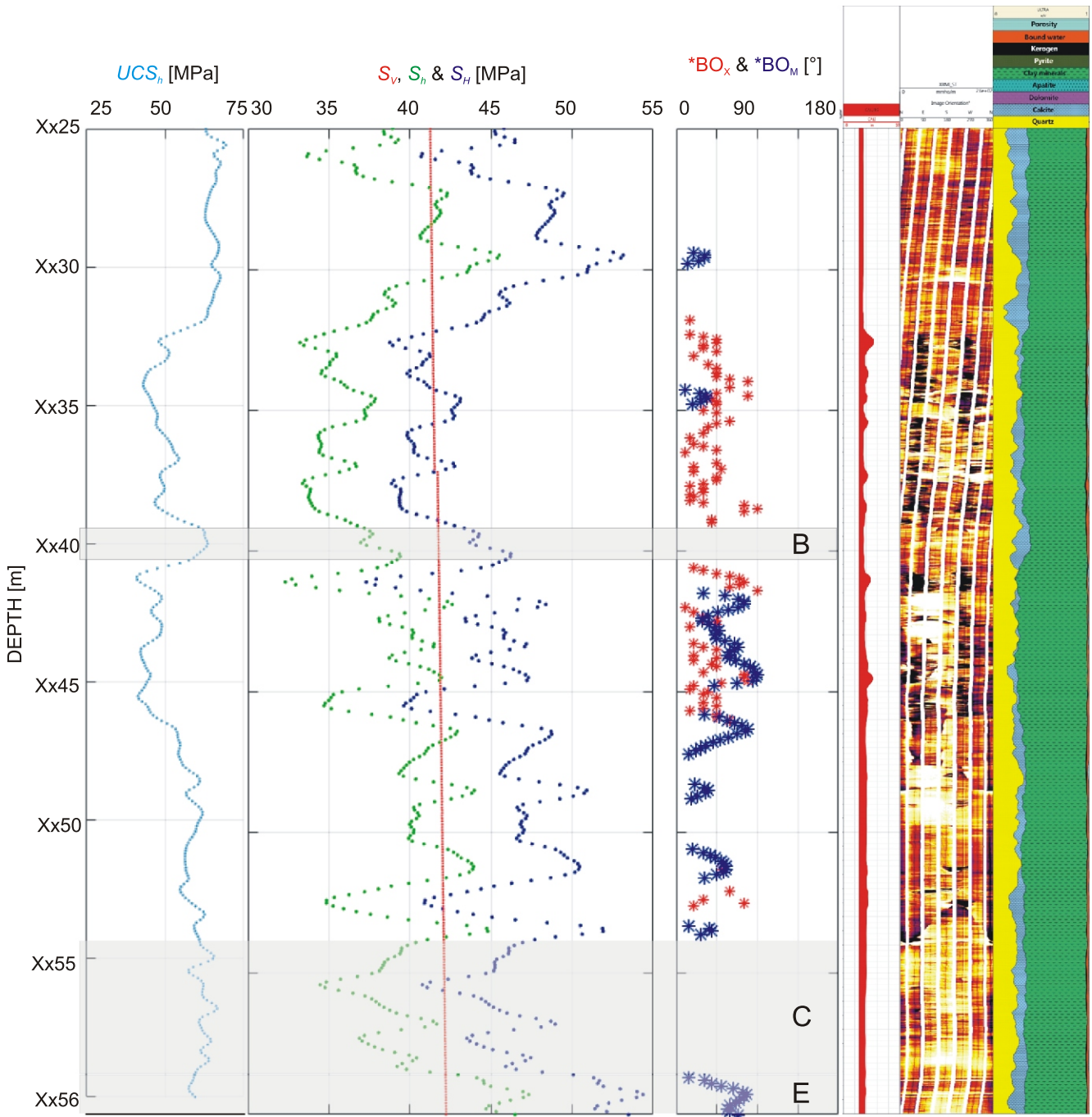
**Fig. 5. Integrated model of strength and stress profiles with observed and modelled breakouts
from the lower selected depth interval**

The first plot shows the USC$_h$ profile for the borehole OX lower test interval with breakouts (lower Puck Formation) as obtained by Wojtowicz et al. (2021). The second plot depicts the S_V profile derived from [eq. 1] and the modelled profile of S_H and S_h estimated using a far-field stress approach, for ε_h = 0.00018 and ε_H = 0.00056. In the third column the observed (BO$_X$) and modelled (BO$_M$) breakouts are shown. The last column consists of caliper and XRMI logs and the lithological profile. The frames show the representative BO$_X$-free and BO$_M$-free intervals B and C and BO$_X$-free interval E where BO$_M$ occur

STRESS MODELS
FOR ALTERNATIVE FAILURE CRITERIA

To further investigate the mechanical conditions of breakout appearance we conducted a stability analysis in BAAR software for the same sections of the OX borehole (upper and lower) as in the previous chapter (Fig. 6). Because we suspect that the mechanical properties within the BO$_X$ sections are disturbed by the presence of borehole wall failure, for the stability analysis we chose BO$_X$-free sections from intervals for which mechanical properties are best constrained (Fig. 6 and Table 1).

Sections A–C are BO$_M$-free, while sections D and E contain BO$_M$. We calculated average magnitudes of elastic parameters, UCS_h, pressure and far-field stresses for each section and ω_{bo}
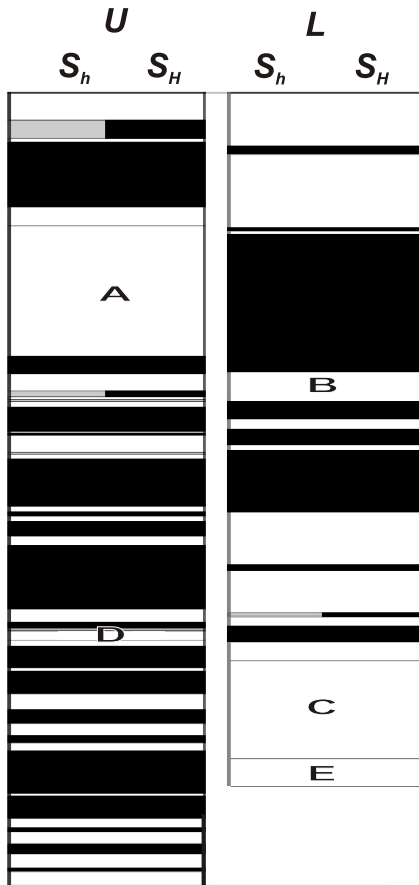
Fig. 6. Changes in the horizontal stress magnitudes in sequences of observed breakouts (BOₓ) for test intervals upper (U) and lower (L), in relation to the average background values

Black fields denote changes unfavourable for breakout formation conditions (lower than background) and grey fields denote favourable changes (higher than background). A, B and C denote representative BO_X-free and BO_M-free sections, while D and E denote representative BO_X-free sections for which BO_M occur

cording to L-D and W-C, S_H should not be increased by >7.5 MPa for A–C and by >1.5 MPa for D and E.

Case 3. We conducted an analysis for BO_X-free sections D and E with modelled BO_M, to obtain S_H magnitudes required for BO_M developed with maximum ω_{bo} as derived from M-C modelling for a given section (Fig. 9 and Table 2). For section D, BO_M with $\omega_{bo} \approx 56°$ developed at S_H ~12% (L-D) or 16% (W-C) higher than estimated by the M-C model. For section E , BO_M with ω_{bo}. 80° developed at S_H ~20% (L-D) or 27% (W-C) higher than estimated by M-C, which indicates a significant discrepancy between criteria incorporating the strengthening effect of σ_{22} and the M-C criterion and possibly an overestimation of rock strength in the case of L-D and W-C.

CORRECTION TO THE FAR-FIELD STRESS MODEL: A DISCUSSION

The horizontal stress profile for the OX borehole was obtained from far-field stress modelling by adjusting the integrated length of BO_X and BO_M and by fitting the modelled DITF to the intervals where these type of fractures are observed. The seemingly good fit between the length and location of BO_X and BO_M at a borehole scale, is shown to be inaccurate in close-up examination of the Puck Formation where breakouts concentrate. BO_X and BO_M zones mostly intertwine, rarely occurring at the same depth. Moreover, modelled horizontal stress changes in the BO_X sections are not consistent with conditions for breakout formation. Since the model was computed using post-drilling data, we concluded that for the BO_X sections, where the mechanical parameters of the rock were already disturbed by breakout formation, the modelled S_h and S_H are not consistent with the stress state prior to drilling. Because of that, the modelled stress regimes for these sections can also differ from the actual state. We observed that BO_X-free sections are mostly in a strike-slip faulting regime, while all BO_X-free sections with BO_M are in a reverse faulting regime.

We decided to test the modelling results by further analysing the BO_X-free sections of which the mechanical parameters are best constrained and to include the strengthening effect of σ_{22} by utilizing L-D and W-C failure criteria. By applying stability analysis to BO_X-free sections using post-drilling parameters and modelled stress, we found that a strengthening effect took place and BO_M did not initiate in BO_X-free sections (Case 1).

We continued the stability analysis for a set S_h profile and concluded that according to L-D and W-C for the BO_X-free sections to remain stable, the S_H should not be increased by more than 1.5 MPa. Because the stability analysis utilized alternative criteria, we cannot directly apply its results to an M-C based

for section D and E (Table 1). Since no hydraulic fracturing data were available for the OX borehole, for the further analysis we assumed that the S_h magnitude profile obtained from the far-field stress modelling is set (Figs. 4 and 5).

Case 1. We applied Lade-Duncan (L-D) and Wiebols-Cook (W-C) failure criteria (Appendixes 2 and 3) in BAAR to sections A–E (Table 1) to include the strengthening effect σ_{22} has on the borehole wall and to compare the results with the stress modelling that was conducted based on the Mohr-Coulomb (M-C) criterion. For all sections, criteria L-D and W-C returned a stable wall, but for sections D and E they indicated a state closer to the failure site (Fig. 7). Therefore we concluded that the results obtained from the L-D and W-C criteria, including the σ_{22} effect, are generally consistent with XRMI observations for A–E, and we continued with the further analysis using these criteria.

Case 2. We investigated the possible upper range of S_H magnitude for BO_X-free sections by estimating the minimal value of S_H required for breakout initiation with L-D and W-C criteria (Fig. 8 and Table 2).

According to L-D and W-C criteria, BO_M would initiate for all intervals at $S_H > S_V$, in a strike-slip faulting regime for BO_X-free and BO_M-free sections (A–C) and in a reverse faulting regime for BO_X-free with BO_M sections (D and E; Table 2). For A–C the required S_H should be ~16.5–24% higher in relation to the far-field stress model relying on the MC, but for D and E, S_H should be only ~2.8–7.7% higher. This, alongside the BO_M occurrence in the M-C model, indicates that sections D and E are closer to the failure site than A–C. For the sections to remain consistent with observations, no BO_M should be initiated, so ac-

Table 1

Average values of mechanical parameters and modelled stresses for selected BO$_X$-free sections (A–E), where *UCS$_h$* denotes unconfined compressive strength in a horizontal direction

Interval	UCS_h [MPa]	E_v [GPa]	E_h [GPa]	ν_v [-]	ν_h [-]	P_f [MPa]	P_p [MPa]	S_V [MPa]	S_h [MPa]	S_H [MPa]	Faulting regime	ω_{bo}[°]
A	55.36	11.18	18.48	0.25	0.31	19.84	18.30	38.30	35.83	41.17	strike–slip	–
B	60.82	14.81	22.69	0.25	0.30	21.34	19.69	41.76	38.03	44.64	strike–slip	–
C	62.07	13.91	23.03	0.24	0.29	21.53	19.86	42.13	38.70	45.49	strike–slip	–
D	52.97	8.13	17.84	0.28	0.27	20.04	18.48	38.69	40.99	46.33	reverse	56
E	59.64	9.39	22.37	0.28	0.23	21.57	19.90	42.21	45.60	52.54	reverse	80

E_v, E_h, ν_v and ν_h are Young's moduli and Poisson ratios in vertical and horizontal directions respectively, P_f and P_p are borehole fluid and pore pressure, S_v, S_h and S_H are vertical, minimum and maximum horizontal far-field stresses and ω_{bo} denotes width of modelled breakouts; sections A–C are BO$_M$-free, and for sections D and E BO$_M$ occur
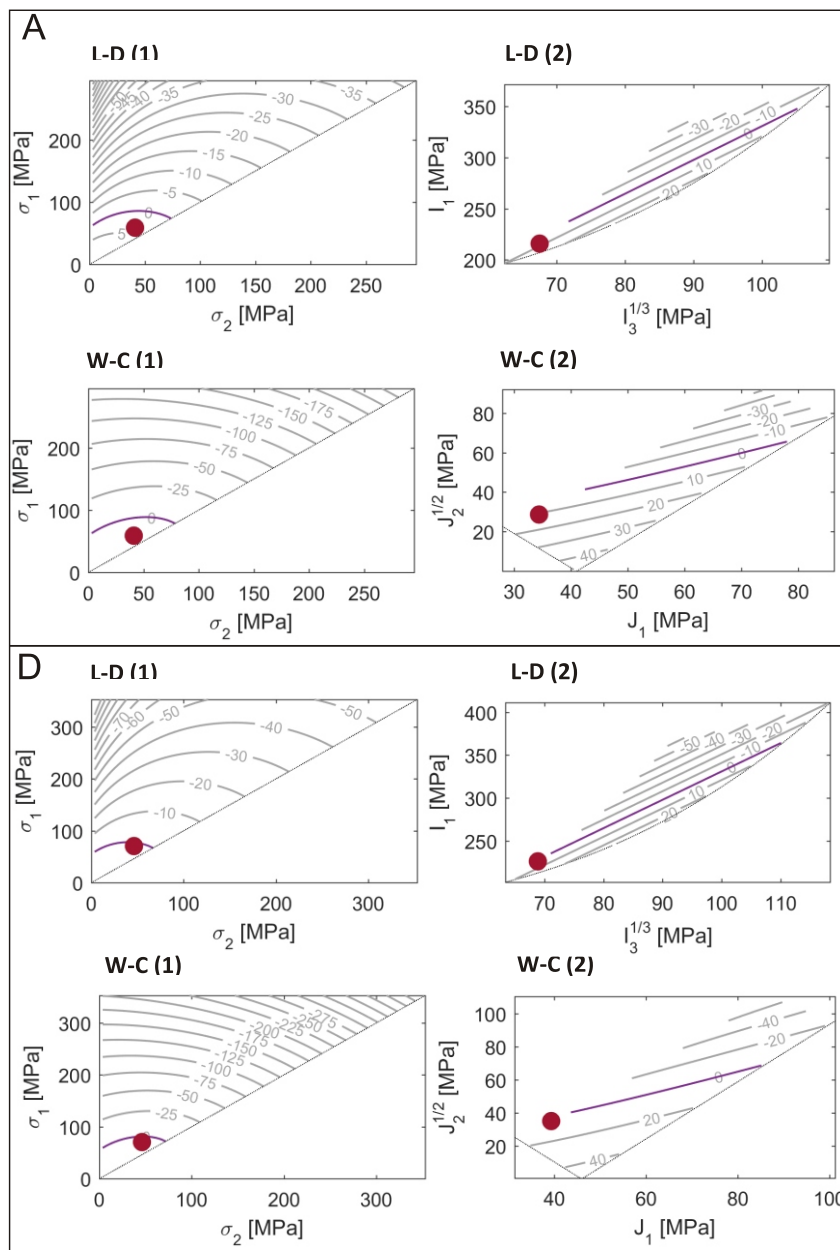

Fig. 7. Stable borehole wall for sections A (representative for A–C) and D (representative for D–E) given by L-D and W-C failure criteria; where (1) denotes the state at point $\theta = \pi/2$ (where $\theta = 0$ is S_H azimuth) shown on $\sigma_1(\sigma_2)$ diagram and (2) denotes the state at point $\theta = \pi/2$ shown on a $I_1(I_3^{1/3})$ diagram for L-D and on a $J_2^{1/2}(J_1)$ diagram for W-C where I_1, I_3, J_1 and J_2 denote stress invariants (Appendixes 2 and 3); positive values refer to the stable area, negative indicate the yield area, and the red dot points to the current state
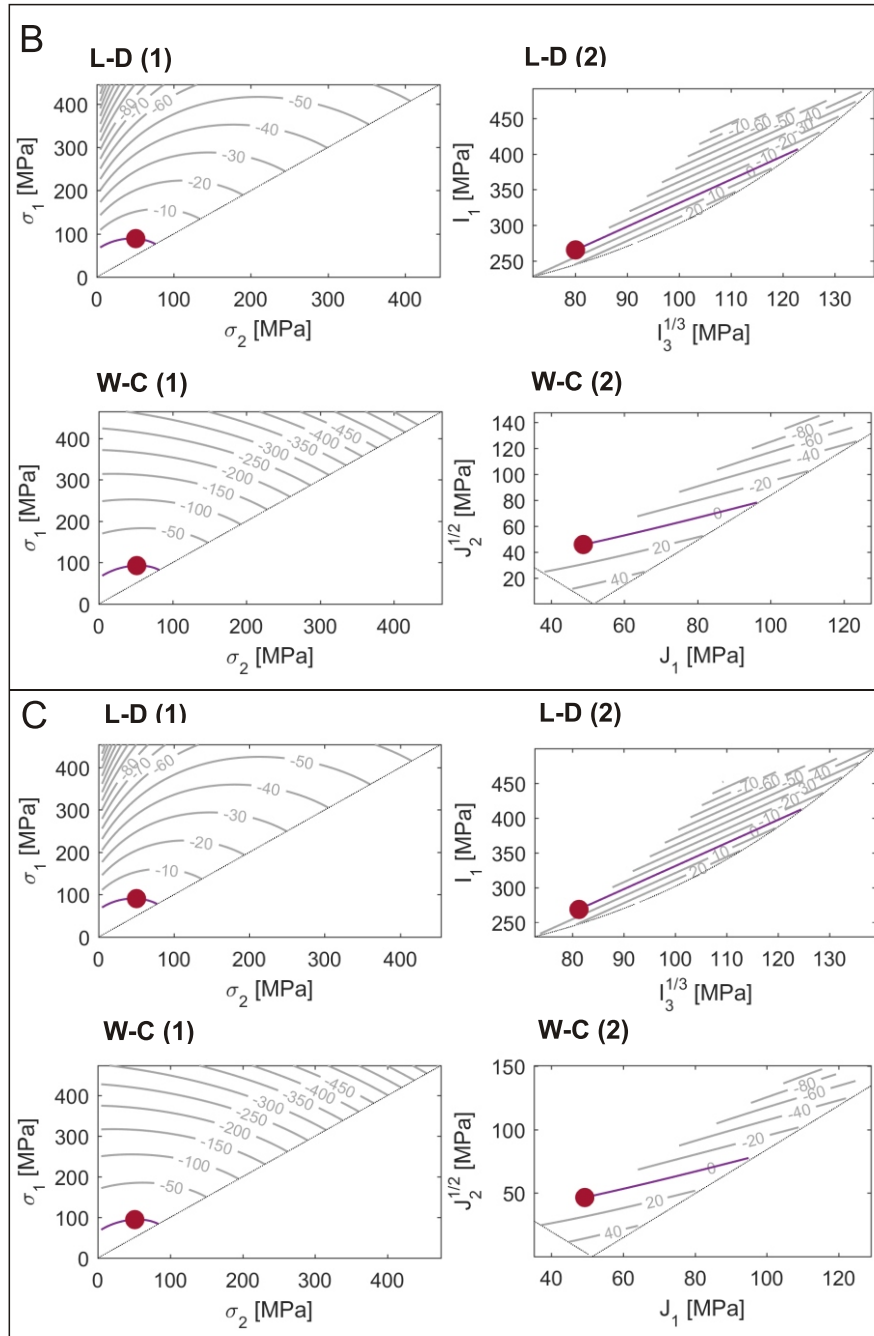
Fig. 8. BO$_M$ initiation for sections B and C (representative for A–E), given by L-D and W-C criteria at the failure site (Table 2)

For other explanations see Figure 7

model. Since both L-D and W-C tend to give higher estimations of rock strength, the above condition should be lowered. This is especially evident for D and E, since according to M-C BO$_M$ already developed in those sections, so S_H should be decreased below the current value. Because of that we recalculated the far-field stress model for the OX borehole to rule out BO$_M$ initiation in BO$_X$-free sections.

By adjusting ε_H and ε_h we computed a horizontal stress profile consistent with a pre-drilling state of stress for stable intervals of the OX borehole. If fracking data was available, restrictions could have been also put on S_h.

Since mechanical parameters for BO$_X$ sections are disturbed, we could not adjust the model to those intervals. Moreover, because the horizontal stresses were decreased to match the stable intervals, the conditions in the BO$_X$ sections were pushed further in the direction of a normal faulting regime. As a result, the density and length of BO$_M$ decreased also in BO$_X$ sections. To accurately model the stress state in BO$_X$ intervals we would need to examine the relations between horizontal stresses and mechanical parameters in BO$_X$ and BO$_X$-free sections and find an appropriate approximation, which is a subject for further investigation. Following the above discussion, we ad-

Table 2

Stress magnitudes and faulting regimes for BO$_X$-free intervals A–E according to the far-field stress model (M-C based), S_H magnitudes for BO$_M$ initiation according to L-D and W-C criteria and S_H magnitudes for BO$_M$ developed at maximum ω_{bo} (as derived from M-C modelling) for intervals D and E according to L-D and W-C

Interval	M-C based model			Faulting regime	L-D	W-C
	S_V [MPa]	S_h [MPa]	S_H [MPa]		S_H [MPa]	S_H [MPa]
	BO$_X$-free & BO$_M$-free			BO$_M$ initiated		
A	38.30	35.83	41.17	strike-slip	50.1	51.1
B	41.76	38.03	44.64	strike-slip	52.1	53.4
C	42.13	38.70	45.49	strike-slip	53.0	54.3
	BO$_X$-free & BO$_M$			BO$_M$ initiated		
D	38.69	40.99	46.33	reverse	48.6	49.9
E	42.21	45.60	52.54	reverse	54.0	55.5
	BO$_X$-free & BO$_M$			BO$_M$ developed		
D	38.69	40.99	46.33	reverse	51.9	53.8
E	42.21	45.60	52.54	reverse	63.0	66.5

justed the model by avoiding BO$_M$ in the places where BO$_X$ are absent. It was obtained, for strains reduced to:

$$_h = 0.00014 \text{ and } _H = 0.00028 \quad [15]$$

for which the BO$_M$ profile received is 7.1 m long. We deem the far-field stress model obtained to be a more precise estimation of the pre-drilling stress state for stable intervals of the OX borehole (Fig. 10).

According to the adjusted model (Fig. 10), the S_H and S_h were decreased in the BO$_X$-free sections of the test intervals (Figs. 4 and 5) by averages of 6.5 and 2.7 MPa respectively. The average differential stress for these sections is equal 2.2 MPa, which is 63% lower in relation to the first model. The upper Puck Formation, with a single BO$_x$, is in the normal faulting stress regime. In the middle Puck Formation, with the majority of BO$_x$, the minimum stress values are artificial disturbed by borehole wall failures. The maximum stress values indicate a strike-slip regime, while the majority of BO$_X$-free sections in the test intervals are subjected to a normal faulting regime. The lowermost part of the Puck Formation is in a reverse faulting regime. The rest of borehole profile is in a normal faulting stress regime with minor exceptions where reverse and strike-slip regimes are present in few-metres-long intervals. The most definite normal faulting stress regime is characteristic of intervals bearing DITF and centerline fractures, in the bottom segment of the borehole (Fig. 10). The average differential stress for the BO$_X$-free interval of the upper Puck Formation located directly above the high BO$_x$ concentration and subjected to a normal faulting regime is 1.7 MPa. For the BO$_X$-free interval located directly below the BO$_x$ concentration, in a predominantly reverse faulting stress regime, the differential stress is equal to 3.1 MPa. For both these intervals, the differential stress is 63.2% lower in relation to the first model. For the Cambrian interval in the deepest normal faulting regime the difference between S_V and S_h is equal to 31.6 MPa, which is 13.9% higher in relation to the first model. With the further adjustment of strain it should be possible to completely remove BO$_M$ from BO$_X$-free

sections and receive a stress profile most consistent with pre-drilling conditions in these sections. It should be noted, though, that due to averaging of multiple parameters, the estimations for both models are of moderate accuracy.

CONCLUSIONS

We modelled the current-state stress profile for the borehole OX, located in the Pomeranian part of the EEC. We studied the interval of the Lower Paleozoic shale successions of the Baltic Basin. The modelling of far-field stresses was conducted based on the theory of elasticity, on account of the VTI symmetry of mechanical properties and utilizing the Mohr-Coulomb failure criterion.

Initial results of our stress modelling revealed a good match of cumulative length of modelled and observed breakouts, as well as a general consistency of breakout development in the Puck Formation and drilling-induced fracture occurrence in the lower part of the borehole profile analysed.

However, when analysing intervals of high breakout concentration, we observed that modelled and observed breakout sections systematically intertwine instead of overlapping. Detailed analysis of selected borehole intervals showed that breakouts developed in places with increased carbonate content. However, in these sections we observed a regular decrease in the horizontal stress values, which theoretically did not favour breakout development. Hence, we concluded that the compressive failure of the borehole wall is the cause of mechanical properties disturbance, which does not allow for reliable modelling of stress and breakouts in those sections.

Analysis of the stress model sensitivity to alternative failure criteria showed that, for the Lade-Duncan and Wiebols-Cook criteria, we obtain a strengthening of the borehole wall by at least 1.5 MPa, which should translate into a similar increase in differential stress profile in relation to the Mohr Coulomb-based model. Determining that the magnitudes of stresses in the sections with observed breakouts are artificially distorted,
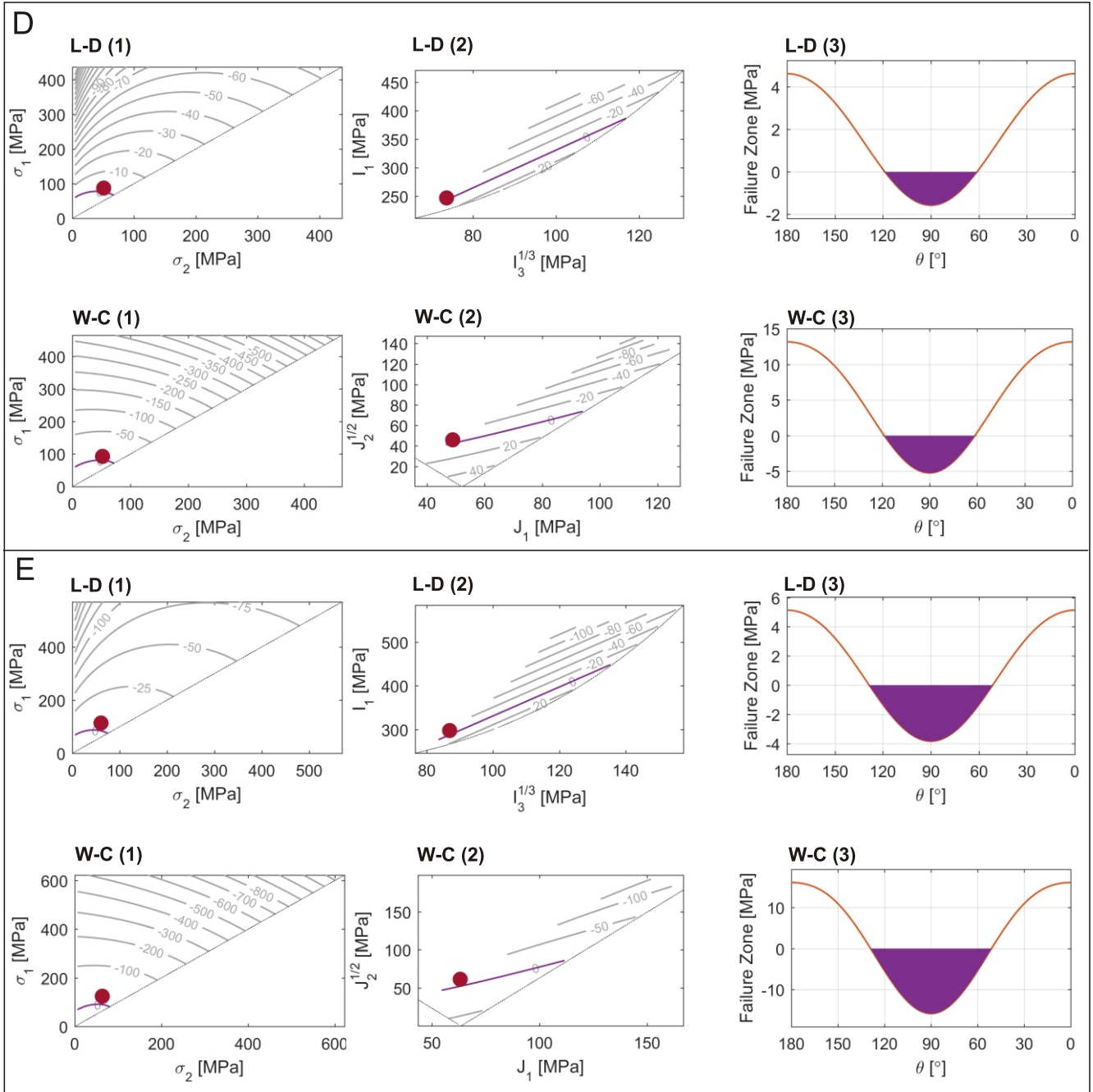
Fig. 9. Developed BO$_M$ with maximum $\omega_{bo} \approx 56°$ and 80° respectively for sections D and E, given by L-D and W-C criteria (Table 2)

For other explanations see Figure 7

prompted us to modify the initial stress model so that modelled breakouts did not occur in the intervals without observed breakouts.

For this, in our opinion, the most reliable solution we obtained had, as expected, a significant mismatch in the total length of the modelled and observed breakouts (7.1 and 99 m respectively). For this solution, the borehole intervals without observed breakouts are located predominantly in a normal faulting stress regime, except for the lower part of the Puck Formation, where a reverse faulting stress regime prevails. Drilling-induced tensile fractures occur in the lower part of the bore-

hole profile where horizontal stress values are the lowest. The interval where breakouts occur (excluding sections disturbed by the presence of breakouts) is in a strike-slip stress regime. We conclude that the breakout sections should also be in a strike-slip or even a reverse faulting stress regime. For the intervals not disturbed by breakouts in the Puck Formation, we obtained values of horizontal differential stresses varying from around 1.7 to 3.1 MPa. We conclude that the modelling of stress profiles in shales should include a detailed and critical analysis of breakout initiation conditions and breakout influence on the rock mechanical properties.
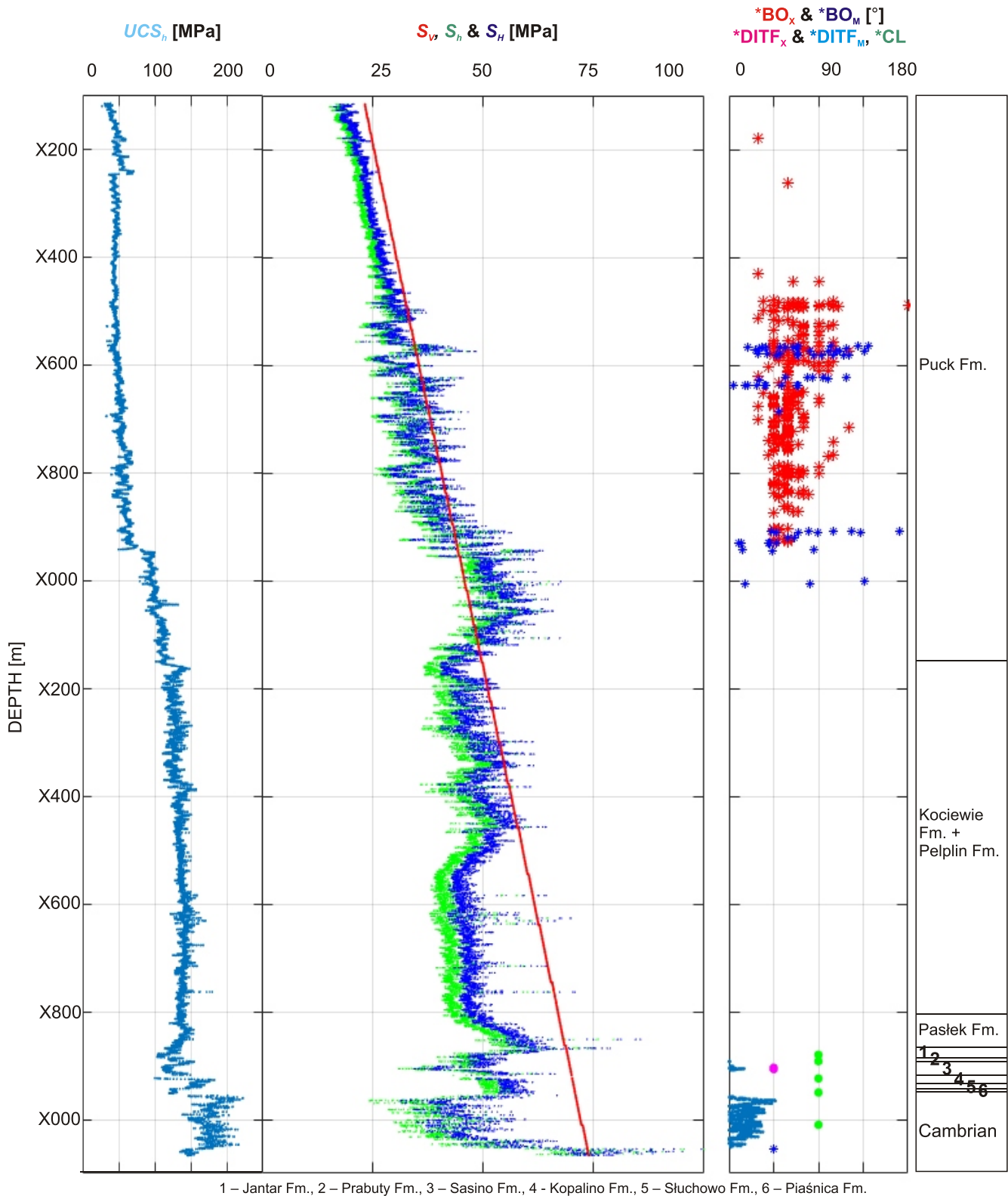
1 – Jantar Fm., 2 – Prabuty Fm., 3 – Sasino Fm., 4 - Kopalino Fm., 5 – Słuchowo Fm., 6 – Piaśnica Fm.

Fig. 10. Stress profiles for the borehole OX obtained by removing BO$_M$ from BO$_X$ sections

The first plot shows the USC$_h$ profile as obtained by Wojtowicz et al. (2021). The second plot depicts the S$_V$ profile derived from [eq. 1] and the adjusted modelled profile of S$_H$ and S$_h$ estimated for BO$_X$-free sections using a far-field stress approach, for ε$_h$ = 0.00014 and ε$_H$ = 0.00028. In the last column the observed (BO$_X$) and modelled (BO$_M$) breakouts, observed (DITF$_X$) and modelled (DITF$_M$) drilling-induced tensile fractures, and centerline fractures (CL), are shown

REFERENCES

Barton, C.A., Zoback, M.D., Burns, K.L., 1988. In-situ stress orientation and magnitude at the Fenton geothermal site, New Mexico, determined from wellbore breakouts. Geophysical Research Letters, **15**: 467–470.

Benz, T., Schwab, R., 2008. A quantitative comparison of six rock failure criteria. International Journal of Rock Mechanics and Mining Sciences, **45**: 1176–1186.

Bobek, K., Jarosiński, M., 2018. Parallel structural interpretation of drill cores and microresistivity scanner images from gas-bearing shale (Baltic Basin, Poland). Interpretation, **6**: 1–50.

Bogdanova, S.V., Bingen, B., Gorbatschev, R., Kheraskova, T.N., Kozlov, V.I., Puchkov, V.N., Volozh, Y.A., 2008. The East European Craton (Baltica) before and during the assembly of Rodinia. Precambrian Research, **160**: 23–45.

Botor, D., Golonka, J., Anczkiewicz, A.A., Dunkl, I., Papiernik, B., Zając, J., Guzy, P., 2019. Burial and thermal history of the Lower Palaeozoic petroleum source rocks at the SW margin of the East European Craton (Poland). Annales Societatis Geologorum Poloniae, **89**: 121–152.

Colmenares, L.B., Zoback, M.D., 2002. A statistical evaluation of intact rock failure criteria constrained by polyaxial test data for five different rocks. International Journal of Rock Mechanics and Mining Sciences, **39**: 695–729.

Dadlez, R., Feldman-Olszewska, A., Gaździcka, E., Iwanow, A., Kiersnowski, H., Leszczyński, K., Marek, S., Pokorski, J., Wagner, R., Wybraniec, S., 1998. Palaeogeographical Atlas of the Epicontinential Permian and Mesozoic in Poland, 1:2 500 000. Wydawnictwo Kartograficzne Polskiej Agencji Ekologicznej SA, Warszawa.

Fjær, E., Holt, R.M., Horsrud, P., Raaen, A.M., Risnes, R., 2008. Petroleum Related Rock Mechanics 2nd ed. Elsevier, Amsterdam.

Gregersen, S., Wiejacz, P., Dębski, W., Domanski, B., Assinovskaya, B., Guterch, B., Mäntyniemi, P., Nikulin, V.G., Pacesa, A., Puura, V., Aronov, A.G., Aronova, T.I., Grnthal, G., Husebye, E.S., Sliaupa, S., 2007. The exceptional earthquakes in Kaliningrad district, Russia on September 21, 2004. Physics of the Earth and Planetary Interiors, **164**: 63–74.

Grüthal, G., Stromeyer, D., Wylegalla, K., Kind, R., Wahlström, R., Yuan, X., Bock, G., 2008. The M_w 3.1–4.7 earthquakes in the southern Baltic Sea and adjacent areas in 2000, 2001 and 2004. Journal of Seismology, **12**: 413–429.

Higgings, S., Goodwin, S., Donald, Q., Donald, A., Bratton, T., Tracy, G., 2008. Anisotropic stress models improve completion design in the Baxter shale. In: Proceedings of SPE ATCE, Denver, 21–24 September, SPE 115736.

Jaeger, J.C., Cook, N.G.W., Zimmerman, R.W., 2007. Fundamentals of Rock Mechanics, Fourth Edition. Blackwell Publishing, Oxford.

Jarosiński, M., 2005. Ongoing tectonic reactivation of the Outer Carpathians and its impact on the foreland: results of borehole breakout measurements in Poland. Tectonophysics, **410**: 189–216.

Jarosiński, M., 2006. Recent tectonic stress field investigations in Poland: a state of the art. Geological Quarterly, **50** (3): 303–321.

Jarosiński, M., Beekman, F., Bada, G., Cloetingh, S., 2006. Redistribution of recent collision push and ridge push in Central Europe: insights from FEM modelling. Geophysical Journal International, **167**: 860–880.

Lekhnitskii, S.G., 1968. Anisotropic Plates. Gordon and Breach, New York.

Matyja, H., 2006. Stratigraphy and facies development of Devonian and Carboniferous deposits in the Pomeranian Basin and in the western part of the Baltic Basin and palaeogeography of the northern TESZ during Late Palaeozoic times (in Polish with English summary). Prace Państwowego Instytutu Geologicznego, **186**: 79–122.

Mavko, G., Mukerji, T., Dvorkin, J., 2009. Rock Physics Handbook: Tools for Seismic Analysis in Porous Media. Cambridge University Press.

Mazur, S., Mikołajczak, M., Krzywiec, P., Malinowski, M., Lewandowski, M., Buffenmyer, V., 2016. Pomeranian Caledonides, NW Poland – a collisional suture or thin-skinned fold-and-thrust belt? Tectonophysics, **692**: 29–43.

Modliński, Z., Podhalańska, T., 2010. Outline of the lithology and depositional features of the lower Palaeozoic strata in the Polish part of the Baltic region. Geological Quarterly, **54** (1): 109–121.

Modliński, Z., Jaworowski, K., Miłaczewski, L., Pacześna, J., Podhalańska, T., Sikorska, M., Szymański, B., Waksmundzka, M.I., 2010. Paleogeological Atlas of the Sub-Permian Paleozoic of the East European Craton in Poland and Neighbouring Areas, 1:2 000 000. Polish Geological Institute – National Research Institute.

Muller, B., Zoback, M.L., Fuchs, K., Mastin, L., Gregersen, S., Pavoni, N., Stephansson, O., Ljunggren, C., 1992. Regional patterns of tectonic stress in Europe. Journal of Geophysical Research, **97**: 11783–11803.

Nowacki, W., 1970. Teoria sprężystości (in Polish). Państwowe Wydawnictwo Naukowe, Warszawa.

Peška, P., Zoback, M.D., 1995. Compressive and tensile failure of inclined well bores and determination of in situ stress and rock strength. Journal of Geophysical Research, **100**: 12791–12811.

Piłacik, A., Adamuszek, M., Dąbrowski, M., 2017. Breakout Analysis for Anisotropic Rocks (BAAR): MATLAB-Based Code to Study Failure Zone Development Around Boreholes in Anisotropic Shales. 51st U.S. Rock Mechanics/Geomechanics Symposium, San Francisco.

Poprawa, P., 2020. Lower Paleozoic oil and gas shale in the Baltic-Podlasie-Lublin Basin (central and eastern Europe) – a review. Geological Quarterly, **64** (3): 515–566.

Poprawa, P., Šliaupa, S., Stephenson, R., Lazauskienė, J., 1999. Late Vendian – Early Palaeozoic tectonic evolution of the Baltic Basin: regional tectonic implications from subsidence analysis. Tectonophysics, **314**: 219–239.

Savin, G.N., 1970. Stress Distribution Around Holes. NASA Technical Translation, NASA TT F-607.

Sone, H., Zoback, M.D., 2013. Mechanical properties od shale-gas reservoir rocks – part 1: Static and dynamic elastic properties and anisotropy. Geophysics, **78**: D381–D392.

Stadtmüller, M., Lis-Śledziona, A., Słota-Valim, M., 2017. Petrophysical and geomechanical analysis of the Lower Paleozoic shale formation, North Poland. Interpretation, **6**: 1–51.

Suarez-Rivera, R., Bratton, T., 2012. Estimating Horizontal Stress from Three-Dimensional Anisotropy. US patent No. 8,175,807 B2.

Thiercelin, M.J., Plumb, R.A., 1994. A core-based prediction of lithologic stress contrasts in East Texas Formations. SPE Formation Evaluation, **9**: 251–258.

Tingay, M., Reinecker, J., Muller, B., 2008. Borehole breakout and drilling-induced fracture analysis from image logs. World Stress Map Project, Guideline: Image Logs.

Vernik, L., Milovac, J., 2011. Rock physics of organic shales. The Leading Edge, **30**: 318–323.

Wang, Y., Dusseault, M.B., 1995. Response of a circular opening in a friable low-permeability medium to temperature and pore pressure changes. International Journal for Numerical and Analytical Methods in Geomechanics, **19**: 157–179.

Wilczyński, P.M., Domonik, A., Łukaszewski, P., 2021. Anisotropy of strength and elastic properties of Lower Paleozoic Shales from the Baltic Basin, Poland. Energies, **14**: 2995.

Wojtowicz, M., Jarosiński, M., 2019. Reconstructing the mechanical parameters of a transversely-isotropic rock based on log and incomplete core data integration. International Journal of Rock Mechanics and Mining Sciences*,* **115**: 111–120.

Wojtowicz, M., Jarosiński, M., Pachytel, R., 2021. Unconfined compressive strength of the Lower Paleozoic shales from the Baltic Basin (northern Poland). Geological Quarterly, **65** (2): 33.

Zhang, L., Cao, P., Radha, K.C., 2010. Evaluation of rock strength criteria for wellbore stability analysis. International Journal of Rock Mechanics and Mining Sciences, **47**: 1304–1316.

Zoback, M.D., 2007. Reservoir Geomechanics. Cambridge University Press.

Zoback, M.D., Moos, D., Mastin, L., Anderson, R.N., 1985. Well bore breakouts and in situ stress. Journal of Geophysical Research, **90**: 5523–5530.

Zoback, M.L., 1992. First- and second-order patterns of stress in lithosphere: the World Stress Map Project. Journal of Geophysical Research, **97**: 11703–11728.